Flux Coupling in the Human Serotonin Transporter

Scott V. Adams* and Louis J. DeFelice†
*Department of Physics and Astronomy and †Department of Pharmacology, Vanderbilt University, Nashville Tennessee 37232 USA

ABSTRACT The serotonin (5-hydroxytryptamine; 5HT) transporter (SERT) catalyzes the movement of 5HT across cellular membranes. In the brain, SERT clears 5HT from extracellular spaces, modulating the strength and duration of serotonergic signaling. SERT is also an important pharmacological target for antidepressants and drugs of abuse. We have studied the flux of radio-labeled 5HT through the transporter stably expressed in HEK-293 cells. Analysis of the time course of net transport, the equilibrium 5HT gradient sustained, and the ratio of the unidirectional influx to efflux of 5HT indicate that mechanistically, human SERT functions as a 5HT channel rather than a classical carrier. This is especially apparent at relatively high $[5HT]_{out}$ ($\geq$10 μM), but is not restricted to this regime of external 5HT.

INTRODUCTION

Sodium-coupled transport across cell membranes occurs via specialized integral membrane proteins called co-transporters or secondary transporters (Stein, 1986; Läuger, 1991). Several different gene families comprise co-transporters, and here we examine a member of the GAT/NET Na/Cl coupled co-transporter family, the human serotonin transporter (hSERT) (Ramamoorthy et al., 1993). hSERT modulates serotonergic signaling in the nervous system (Iversen, 1971; Bunin and Wightman, 1998) and is implicated in human behaviors such as mood, appetite, and sexual behavior. Serotonin-selective reuptake inhibitors, which block hSERT and 5-hydroxytryptamine (5HT) uptake, are used to treat depression, panic disorders, and premenstrual dysphoric syndrome (Ramamoorthy et al., 1993; Tatsumi et al., 1997; Parry, 2001). hSERT is also a receptor for psychostimulants such as 3,4-methylenedeoxymethamphetamine (MDMA, "ecstasy"), amphetamine, and cocaine (Blakely et al., 1991; Rudnick and Wall, 1992; Ramamoorthy et al., 1993; Johnson et al., 1998).

hSERT not only transports 5HT but can concentrate 5HT against its electrochemical gradient by utilizing energy stored in the ionic gradients of sodium, chlorine, and potassium (Keyes and Rudnick, 1982; Gu et al., 1994a,b). Coupled transport is usually visualized as an enzymatic cycle in which 5HT, sodium and other ions bind to the outer face of the transporter and induce a conformational change that ultimately deposits the co-ligands inside the cell. In this scheme, illustrated in Fig. 1*A*, hSERT actively mediates the transfer of energy from ion gradients (typified by sodium) to the substrate gradient (5HT), through conformational changes. If the net transfer of charge is zero, as proposed for some 5HT transporters (Rudnick and Nelson, 1978; Gu et al., 1994a), the transport cycle is referred to as electroneutral.

An alternative mechanism for coupled transport is that 5HT and sodium permeate a narrow pore through the SERT protein, and that coupling between ion and substrate results from queuing of the co-permeating species. Previous evidence suggests that a channel model may be appropriate for the Na/Cl coupled GAT/NET gene family (Su et al., 1996; Galli et al., 1996, 1997; Petersen and DeFelice, 1999). In our model, illustrated in Fig. 1, *B* and *C*, coupling would not occur if ions freely passed one another. Single-file diffusion of ions and substrate can, however, reproduce several critical features of coupled transport, including transport of substrate against its electrochemical gradient and amplification of ion gradients into the substrate gradient by a power law. The inspiration for our model comes from studies of potassium channels. Almost fifty years ago, Hodgkin and Keynes (1955) observed that the flux of potassium through the squid axon deviated from Ussing's Law, and they described the deviation in terms of a single-file, knock-through model. The fundamental feature of their model as a narrow multi-ion pore is now verified with the structural determination of the bacterial potassium channel Kcsa (Doyle et al., 1998). In the intervening time, numerous biophysical experiments have supported Hodgkin and Keynes' model (Hille and Schwarz, 1978), and single-file diffusion is a framework for understanding permeation through many different ion channels (Hille, 2001).

We have extended the Hodgkin and Keynes model to include the possibility of different ionic species permeating a common pore (DeFelice and Adams, 2001; DeFelice et al., 2001) and searched for qualitative differences that distinguish the channel model of coupled transport from the enzymatic model. Our measurements of 5HT flux through hSERT expressed in a heterologous expression system are more closely described by a channel mechanism of permeation and coupling and not by the enzymatic model.

THEORY

Classical enzymatic coupling model

Before considering the kinetics of the scheme in Fig. 1 *A*, we review the thermodynamics of stoichiometric co-transport. For simplicity, we confine ourselves to 5HT and sodium and

Submitted May 20, 2002 and accepted for publication August 8, 2002.

Address reprint requests to Louis J. DeFelice, Ph.D., Dept. of Pharmacology, Vanderbilt University Medical Center, Nashville, TN 37232-6600. Tel.: 615-343-6278; Fax: 615-343-1679; E-mail: lou.defelice@mcmail.vanderbilt.edu.

© 2002 by the Biophysical Society

0006-3495/02/12/3268/15 $2.00

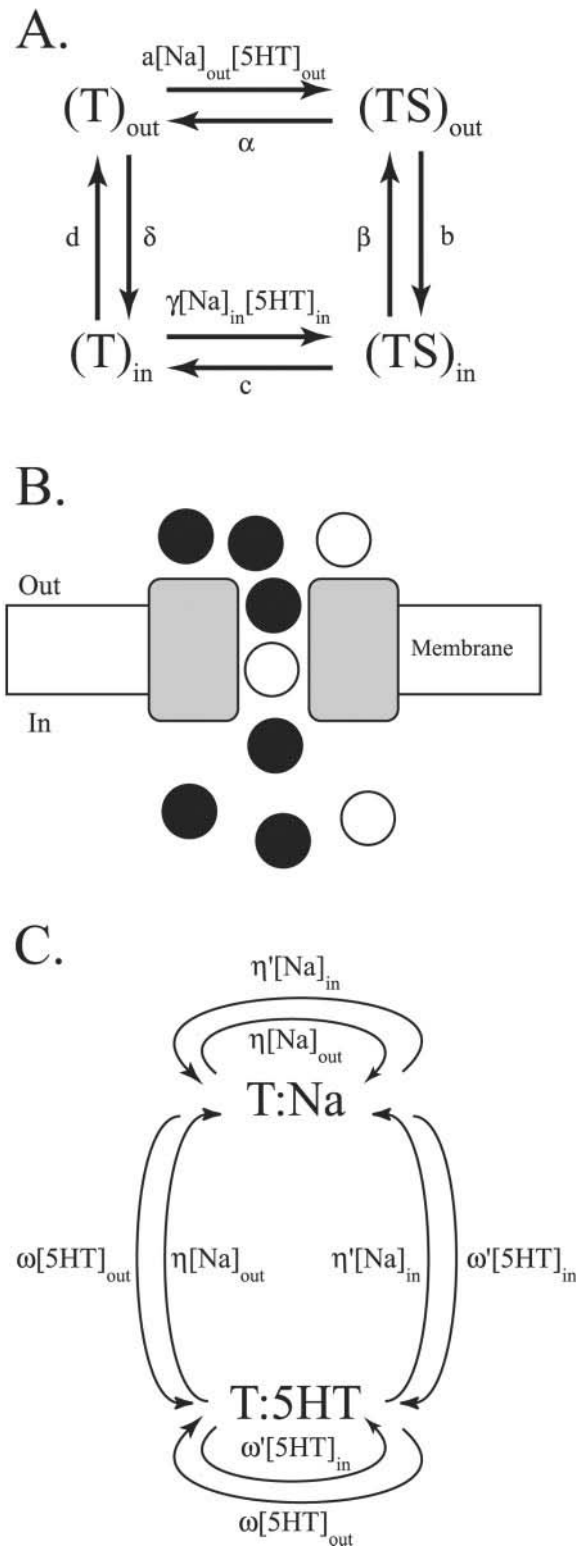

FIGURE 1 Models of sodium-coupled 5HT transport through hSERT. (*A*) Enzymatic cycle model, in which the transporter T cycles between outward and inward facing states. *S* represents the substrates, *m* sodium ions and one 5HT molecule. (*B*) Single-file pore model, in this case with $n = 2$ sites which may each be occupied by either 5HT or sodium. Ions move in the pore when an ion enters from either face, in a knock-through fashion. (*C*) Kinetic scheme for a pore with $n = 1$ site for either sodium or 5HT. The various rate steps represent sodium or 5HT entering from the internal or external side of the pore.

consider only the chemical driving force, but the results are easily generalized to other ions and to include voltage. The equilibrium condition of the chemical free energy during one transport cycle, in which *m* sodium ions are transported with each 5HT ion, yields the well-known result for the equilibrium gradient of 5HT as a function of the existing and constant sodium gradient,

$$\frac{[5HT]_{in}}{[5HT]_{out}} = \left(\frac{[Na]_{out}}{[Na]_{in}}\right)^{m}. \tag{1}$$

The 5HT equilibrium gradient does not depend on the microscopic rate constants in the transport scheme. Importantly, the 5HT equilibrium gradient does not depend on the magnitude of internal or external 5HT concentration; thus a 10-fold higher $[5HT]_{out}$ leads to a 10-fold higher $[5HT]_{in}$ at equilibrium, as long as the sodium gradient remains constant. Any stoichiometric transport scheme, without substrate slippage, must produce Eq. 1 when equilibrium conditions are applied to kinetic equations.

Now we turn to the model pictured in Fig. 1 *A*, which consists of four transporter states connected by rate constants. Because we are considering only sodium and 5HT, only two steps in the cycle depend upon substrate or ionic concentrations. Extensions to this basic scheme are numerous and well known (Stein, 1986). To analyze the enzymatic model, we use the familiar King–Altman diagrammatic method (King and Altman, 1956) to obtain expressions for the unidirectional influx and efflux. Here we only sketch the procedure, because it is well known and appears in many textbooks and monographs (Stein, 1986). For unidirectional influx, a unique series of transitions must occur among the transporter states. First, substrates must bind to the outward-facing transporter $(T)_{out}$, the transporter then reorients itself, and the substrates release into the internal compartment. This sequence of transitions occurs with a rate given by

$$\phi_{in} = a[Na]_{out}^{m}[5HT]_{out}(T)_{out}\left(\frac{b}{b+\alpha}\right)\left(\frac{c}{c+\alpha\beta/(b+\alpha)}\right). \tag{2}$$

ϕ_{in} is the rate of transport of *m* sodium for each 5HT from out to in. Similarly, unidirectional efflux is given by

$$\phi_{out} = \gamma[Na]_{in}^{m}[5HT]_{in}(T)_{in}\left(\frac{\beta}{c+\beta}\right)\left(\frac{\alpha}{\alpha+bc/(c+\beta)}\right). \tag{3}$$

Thus the flux ratio can be simplified to

$$\frac{\phi_{out}}{\phi_{in}} = \frac{\alpha\beta\gamma[Na]_{in}^{m}[5HT]_{in}(T)_{in}}{abc[Na]_{out}^{m}[5HT]_{out}(T)_{out}}. \tag{4}$$

The King–Altman diagrammatic method can now be used to directly calculate the state populations $(T)_{in}$ and $(T)_{out}$ in terms of the microscopic rate constants and substrate concentrations. In this approach, a diagram is made for every combination of three transitions that lead to the state of interest, each representing the product of the rate constants for these three transitions. The diagrams are summed, resulting in the fractional occupation of the states,

$$\frac{(T)_{in}}{N} \propto abc[Na]^m_{out}[5HT]_{out} + \delta(\alpha\beta + bc + c\alpha) \quad (5)$$

and

$$\frac{(T)_{out}}{N} \propto \alpha\beta\gamma[Na]^m_{in}[5HT]_{in} + d(\alpha\beta + bc + c\alpha). \quad (6)$$

Here N represents the total (fixed) number of transporter proteins. The constant of proportionality missing from both Eqs. 5 and 6 is equal to the sum of the equivalent expression for each of the states in Fig. 1 *A*. In a probabilistic interpretation, the proportionality constant normalizes the state populations.

After some rearrangement, the flux ratio is given by

$$\frac{\phi_{out}}{\phi_{in}} = \frac{\alpha\beta\gamma\delta[Na]^m_{in}[5HT]_{in}}{abcd[Na]^m_{out}[5HT]_{out}} \times \left(\frac{abcd[Na]^m_{out}[5HT]_{out} + d\delta(\alpha\beta + bc + c\alpha)}{\alpha\beta\gamma\delta[Na]^m_{in}[5HT]_{in} + d\delta(\alpha\beta + bc + c\alpha)}\right). \quad (7)$$

Eq. 7 is the complete expression for the flux ratio of 5HT co-transported with m sodium ions, but it can be simplified further. At equilibrium, the flux ratio must be equal to one. Imposing this condition on Eq. 7 and using the thermodynamic result Eq. 1 yields the condition

$$abcd = \alpha\beta\gamma\delta. \quad (8)$$

Because all of the factors in Eq. 8 are constants, Eq. 8 must hold true even away from equilibrium. Eq. 8 is often referred to as the "Principle of Detailed Balance." These conditions reduce Eq. 7 to

$$\frac{\phi_{out}}{\phi_{in}} = \frac{[Na]^m_{in}[5HT]_{in}}{[Na]^m_{out}[5HT]_{out}}\left(\frac{[Na]^m_{out}[5HT]_{out} + K}{[Na]^m_{in}[5HT]_{in} + K}\right), \quad (9)$$

where $K = \delta(\alpha\beta + bc + c\alpha)/abc$ is a constant that is independent of the substrate concentrations. At equilibrium, the flux ratio represented by Eq. 9 is equal to 1, yielding an explicit equation for the 5HT gradient,

$$\frac{[5HT]_{in}}{[5HT]_{out}} = \left(\frac{[Na]_{out}}{[Na]_{in}}\right)^m. \quad (10)$$

For our purposes, the central equations of the enzymatic cycle model are Eq. 9 for the flux ratio and Eq. 10 for the equilibrium gradient, which is equivalent to the thermodynamic result, Eq. 1. More complex reaction schemes than Fig. 1 *A* are possible, and many have been discussed in the literature (Stein, 1986, Laüger, 1991). Modifications include sequential binding steps, which may be ordered, and the possibility of slippage transitions. Restrictions on binding order change the definition of K in Eq. 9, but they do not alter Eq. 10.

Slippage transitions occur when the transporter allows the passage of one substrate without its co-substrate; for instance, if SERT transports 5HT without a coupled sodium ion. Slippage complicates the analysis, but the form of the flux ratio as a function of $[5HT]_{in}$ and $[5HT]_{out}$ is preserved (Stein, 1986, pp 398–399), although K becomes dependent on [Na], and extra terms are necessary that depend on [Na]. Thus $\tilde{\phi_{out}}/\phi_{in}$ for the enzymatic model with slippage has the same dependence on $[5HT]_{out}$ and $[5HT]_{in}$ as Eq. 9. Although slippage obviously spoils the thermodynamic limit, Eq. 10, the achieved gradient, whatever it might be, is independent of $[5HT]_{out}$. In contrast, as we now show, the single-file channel model predicts that the 5HT gradient depends on $[5HT]_{out}$.

Single-file model

Here we derive formulas for flux through a narrow pore that is permeable to multiple ionic species. A diagram of this mechanism is shown in Fig. 1 *B*, and an equivalent kinetic scheme in Fig. 1 *C*. First we take a heuristic approach to the diagram model (Fig. 1 *B*) and derive equations that describe a single-file pore. Then we examine the kinetic diagram (Fig. 1 *C*) to obtain a similar result with additional molecular constants.

To begin, we assume two classes of permeating ions, sodium and 5HT and again consider only chemical driving forces. The theory assumes an open pore, within which ions move only when another ion enters the pore from either direction. Only these simple knock-through interactions are allowed, as in Hodgkin and Keynes (1955). Consider unidirectional 5HT influx in the diagram Fig. 1 *B*. Influx occurs when a 5HT molecule enters the pore from the external side, which we assume occurs at a rate proportional to $[5HT]_{out}$. To completely transverse a pore that accommodates n ions, the 5HT ion must be displaced n times by either sodium or 5HT entering the pore from the same side. Our central assumption is that these n events occurs at a rate proportional to $([Na]_{out} + [5HT]_{out})$. Therefore,

$$\phi_{in} \propto [5HT]_{out}([Na]_{out} + [5HT]_{out})^n. \quad (11)$$

Note that Eq. 11 is not symmetric with respect to sodium and 5HT. Asymmetry occurs because we have elected to monitor 5HT, not sodium. For 5HT flux to occur, 5HT must enter the pore (the first factor) *and* then sodium *or* 5HT must displace it. Displacements occur n times in any order

(the second factor) for the original 5HT to influx. The expression ([Na] + [5HT]) treats sodium and 5HT equally in terms of entering and permeating the pore. The concentrations that appear in Eq. 10 are thus effective concentrations proportional to the bath concentration.

To make Eq. 11 an equality, we introduce the proportionality factor,

$$\frac{\omega}{([\mathrm{Na}]_{\mathrm{out}} + [\mathrm{Na}]_{\mathrm{in}} + [5\mathrm{HT}]_{\mathrm{out}} + [5\mathrm{HT}]_{\mathrm{in}})^{n+1}}. \quad (12)$$

The constant ω is the intrinsic rate at which ions approach the pore. The denominator represents the sum of all possible ions that may enter the pore. This sum is raised to the $n + 1$ power, because, for unidirectional flux to occur, $n + 1$ total ions must enter. Thus this denominator normalizes Eq. 11 to the total number of possible events that may occur at the mouth of the pore. It is analogous to normalizing the enzymatic model (Eqs. 5 and 6) to the total number of state transitions.

For unidirectional 5HT efflux, change the concentrations in Eq. 10 to internal concentrations, but the proportionality factor (Eq. 12) remains the same. Thus the total net flux of 5HT is

$$\Phi = \frac{\mathrm{d}[5\mathrm{HT}]_{\mathrm{in}}}{\mathrm{d}t} = \omega \frac{[5\mathrm{HT}]_{\mathrm{out}}([\mathrm{Na}]_{\mathrm{out}} + [5\mathrm{HT}]_{\mathrm{out}})^{n} - [5\mathrm{HT}]_{\mathrm{in}}([\mathrm{Na}]_{\mathrm{in}} + [5\mathrm{HT}]_{\mathrm{in}})^{n}}{([\mathrm{Na}]_{\mathrm{out}} + [\mathrm{Na}]_{\mathrm{in}} + [5\mathrm{HT}]_{\mathrm{out}} + [5\mathrm{HT}]_{\mathrm{in}})^{n+1}}, \quad (13)$$

and the unidirectional flux ratio is

$$\frac{\phi_{\mathrm{out}}}{\phi_{\mathrm{in}}} = \frac{[5\mathrm{HT}]_{\mathrm{in}}}{[5\mathrm{HT}]_{\mathrm{out}}} \left(\frac{[\mathrm{Na}]_{\mathrm{in}} + [5\mathrm{HT}]_{\mathrm{in}}}{[\mathrm{Na}]_{\mathrm{out}} + [5\mathrm{HT}]_{\mathrm{out}}} \right)^{n}. \quad (14)$$

channel model

At equilibrium, $\phi_{\mathrm{out}}/\phi_{\mathrm{in}}$, yielding an implicit equation for the 5HT gradient,

$$\frac{[5\mathrm{HT}]_{\mathrm{in}}}{[5\mathrm{HT}]_{\mathrm{out}}} = \left(\frac{[\mathrm{Na}]_{\mathrm{out}} + [5\mathrm{HT}]_{\mathrm{out}}}{[\mathrm{Na}]_{\mathrm{in}} + [5\mathrm{HT}]_{\mathrm{in}}} \right)^{n}. \quad (15)$$

Note that, in the absence of a sodium gradient, ($[\mathrm{Na}]_{\mathrm{out}} = [\mathrm{Na}]_{\mathrm{in}}$), or for a "non-hole", ($n = 0$), Eq. 15 predicts that the channel cannot sustain a [5HT] gradient, as required.

Another approach to the pore model is to draw a kinetic diagram, Fig. 1 *C*. In this single-site pore, as above, we assume that either sodium or 5HT continuously occupies the site. To begin, assume that the pore may be either T:Na or T:5HT. For unidirectional influx, 5HT must enter the pore from the external face, which occurs at the rate $\omega[5\mathrm{HT}]_{\mathrm{out}}$. As before, ω is the intrinsic rate at which 5HT molecules arrive at the mouth of the pore from the external face. Subsequently, either sodium or 5HT entering from the external face will cause 5HT in the pore to exit to the internal milieu. This occurs at a rate proportional to $\omega[5\mathrm{HT}]_{\mathrm{out}} + \eta[\mathrm{Na}]_{\mathrm{out}}$. Thus the total unidirectional influx of 5HT is, for the case $n = 1$,

$$\phi_{\mathrm{in}} = \frac{\omega[5\mathrm{HT}]_{\mathrm{out}}(\omega[5\mathrm{HT}]_{\mathrm{out}} + \eta[\mathrm{Na}]_{\mathrm{out}})}{(\omega[5\mathrm{HT}]_{\mathrm{out}} + \eta[\mathrm{Na}]_{\mathrm{out}} + \omega'[5\mathrm{HT}]_{\mathrm{in}} + \eta'[\mathrm{Na}]_{\mathrm{in}})^{2}}. \quad (16)$$

The denominator is the sum of all possible transitions, and thus serves to normalize the expression appropriately. The flux ratio is therefore

$$\frac{\phi_{\mathrm{out}}}{\phi_{\mathrm{in}}} = \frac{\omega'[5\mathrm{HT}]_{\mathrm{in}}}{\omega[5\mathrm{HT}]_{\mathrm{out}}} \left(\frac{\omega'[5\mathrm{HT}]_{\mathrm{in}} + \eta'[\mathrm{Na}]_{\mathrm{in}}}{\omega[5\mathrm{HT}]_{\mathrm{out}} + \eta[\mathrm{Na}]_{\mathrm{out}}} \right), \quad (17)$$

where the new constants ω' and η' are equivalent to ω and η on the interior face of the pore. These constants reflect factors such as diffusion and binding of 5HT and sodium. Eq. 17 is the same as Eq. 14 with $n = 1$ and the extra rate constants. If we further assume that $\omega = \eta = \omega' = \eta'$, then Eq. 17 and Eq. 14 are identical (for any n including $n = 1$, as in this example). The concentrations in Eq. 17 are the bath concentrations, but those in Eq. 14 represent effective concentrations. Because we do not know and have not attempted to measure the constants ω, ω', η, η', we use Eq.14, keeping in mind that the concentrations are effective. Either expression gives the same qualitative dependence on [5HT] and [Na].

We are now in a position to compare the enzymatic and channel models directly. In contrast to the enzymatic coupling model Eq. 1, the single-file model Eq. 15 suggests that, at high $[5\mathrm{HT}]_{\mathrm{out}}$, the ability of the transporter to generate a large 5HT gradient is compromised. Essentially this occurs because, as the effective concentration of 5HT increases, 5HT molecules permeate the pathway without interacting with sodium. Instead, 5HT may interact with other 5HT molecules and hence traverse the pore uncoupled to sodium. In the single-file model, $[5\mathrm{HT}]_{\mathrm{in}}/[5\mathrm{HT}]_{\mathrm{out}}$ decreases as external 5HT increases. Recall that the enzymatic model, without or with slippage, predicts that the equilibrium gradient is constant as external 5HT increases. The gradient thus provides a qualitative distinction between the coupling mechanisms illustrated in Fig. 1.

The flux ratio also distinguishes the pore and enzyme models. Eq. 14 shows that, in a single-file pore, the flux ratio increases without saturation as $[5HT]_{in}$ increases. The lack of saturation makes physical sense, because flux ratios greater than 1 occur when the transporter mediates net efflux. No "flux ratio" saturation with increasing $[5HT]_{in}$ does not imply no "net transport" saturation (Eq. 13). By taking the ratio of fluxes, effects leading to saturation cancel. Indeed, any process equally required for influx and efflux (e.g., gating) cancel in the flux ratio. In contrast, the enzymatic model flux ratio, Eq. 9, is hyperbolic in $[5HT]_{in}$ and will saturate with increasing $[5HT]_{in}$. In the enzymatic model, gating and permeation are inseparable, and saturation in the flux ratio reflects saturation of transporter binding sites. In the pore model, the flux ratio is purely a permeation parameter.

To highlight further differences, we may expect, under some experimental conditions, that sodium can permeate more freely than 5HT. Hence, in Eq. 14, we may approximate $[Na] \gg [5HT]$ on both sides of the membrane, so that the flux ratio is directly proportional to the 5HT gradient. This approximation should at least hold for unloaded cells ($[5HT]_{in} = 0$) at low $[5HT]_{out}$. At higher $[5HT]_{in}$, we expect the power-law shape of Eq. 14 to become more apparent. The same approach to Eq. 9 yields a different result. For an unloaded cell with small $[5HT]_{in}$, the efflux pathway in Fig. 1 *A* can be neglected compared to influx. This is equivalent to the condition

$$[Na]^{m}_{in}[5HT]_{in} \ll K \ll [Na]^{m}_{out}[5HT]_{out}. \qquad (18)$$

This leaves the flux ratio Eq. 9 independent of the $[5HT]_{out}$, and proportional to $[5HT]_{in}$, for large $[5HT]_{out}$ and small $[5HT]_{in}$. Intuitively, this is justified because the surplus of substrate on the external face drives unidirectional influx at a constant, high rate, with negligible efflux. However, at high $[5HT]_{out}$, the external sites of the classical transporter are saturated, and therefore external 5HT cannot further affect influx. In the pore model, though binding sites may saturate, external 5HT nevertheless affects influx. Thus we anticipate a possible regime in which to distinguish the two models, namely, at high $[5HT]_{out}$.

MATERIALS AND METHODS

Experiments in tissue culture

HEK-293 cells stably expressing hSERT (HEK-hSERT) (Qian et al., 1997) were grown in DMEM supplemented with 10% dialyzed fetal bovine serum (MW cutoff of 10^4 g/mole), 1% Penn/Strep, and 250 mg/L G418 sulfate. Each well of the poly-D-lysine-coated 24-well plates was seeded with 10^5 cells and grown for 3 days under standard conditions (5% CO_2, 37°C). Before each experiment, the cells were visually inspected and found to be more than 75% confluent.

Before beginning an experiment, the medium was removed and the wells washed once in Krebs–Ringers–Hepes buffer (KRH: 120 mM NaCl, 4.7 mM KCl, 10 mM Hepes, 1.2 mM $MgSO_4$, 1.2 mM KH_2PO_4, 5 mM Tris, 2.2 mM $CaCl_2$) at room temperature. To each well was added 475 μl KRH buffer, supplemented with 1.8 g/L glucose (gKRH). For experiments in which cells were treated with drugs in addition to 5HT, the cells were preincubated with the drugs for at least 20 min before the addition of the 5HT-containing cocktail. All experiments were performed at room temperature (22°C), and experimental baths contained 50 μM ascorbic acid and 50 μM pargyline, to help prevent degradation of 5HT.

At the end of an experiment, cells were lysed with 500 μl 1% SDS, transferred to a scintillation vial, and 3 ml scintillation fluid (Ecoscint, National Diagnostics, Atlanta, GA) was added. The activity of each vial was counted on a Wallac 1209 RackBeta liquid scintillation counter (Perkin Elmer, Boson, MA). Counts per minute (cpm) were converted to picomoles of 5HT by counting an aliquot of the experimental cocktail (with 500 μl 1% SDS and 3 ml scintillation fluid) to determine pmole 5HT per cpm. Following each experiment, we trypsinized 12 wells of an identically cultured plate of cells, and counted the cells/well using a hemocytometer. Typical values were between 3.5×10^5 and 6×10^5 cells/well. Assuming a volume of 1.25 pl/cell, we calculated $[5HT]_{in}$ and flux/cell for each experiment.

Experiments were performed such that all cells were at room temperature and incubated in gKRH for approximately the same time. Furthermore, experiments were paired such that each experiment at 30, 1, or 0.1 μM was done in parallel with an experiment at 10 μM 5HT. Therefore, each experiment was compared directly to an experiment at 10 μM $[5HT]_{out}$ to insure that differences in uptake are not the result of difference in cell-culture conditions or other uncontrolled variables. Finally, unidirectional influx and net flux time course experiments were performed at the same time, in parallel, on the same plates of cells.

Net uptake and gradient

The experiment began with the addition of 25 μl cocktail to the well. The cocktail contained [5HT] such that the bath concentration was as indicated. For uptake time course experiments (Fig. 2, *A* and *B*), a small constant fraction of this 5HT (0.1%) was [^{3}H]-5HT, so that net uptake could be determined from uptake of radiolabeled substrate.

At the indicated time, the experimental buffer was removed from the well, and the cells washed twice with 250 μl ice-cold KRH buffer to stop transport. Each net uptake time course experiment consisted of four experimental wells and two citalopram-treated control wells at each indicated time point. Specific uptake was defined as the difference between wells preteated (5–10 min) with 100 μM citalopram and untreated wells.

The 5HT gradient after 81 min of uptake was also measured for many $[5HT]_{out}$ (Fig. 2 *C*). For these two experiments, the fraction of [^{3}H]-5HT in the bath was 6.4×10^{-5} for 100 μM $\geq [5HT]_{out} >$ 30 μM; 1.6×10^{-3} for 10 μM $\geq [5HT]_{out} >$ 1 μM; or 9.8×10^{-3} for $[5HT]_{out} <$ 0.3 μM. For each $[5HT]_{out}$, uptake was measured in three duplicate wells, in addition to one well pretreated with 750 μM citalopram.

Unidirectional influx

For the measurement of unidirectional influx, the cells were first loaded with unlabeled (cold) 5HT. The bath concentration in this case was 30, 10, 1, or 0.1 μM. Thus, these cells were loaded in parallel with the uptake time course cells, but contained no labeled 5HT. The unlabeled and labeled loading cocktails were always made from a common 5HT stock.

At the indicated time, a small amount (5 or 7.5 μl) of challenge cocktail was added to the bath of the cold-loaded cell. This brought the [^{3}H]-5HT concentration in the well to 20 nM, for cells loaded at 30 or 10 μM total [5HT], or 15 nM, for cells loaded at 1 or 0.1 μM. The cells were incubated in this solution for 1 min, and then the buffer was removed and the cells were washed twice with 250 μl ice-cold KRH buffer. The 5HT accumu-

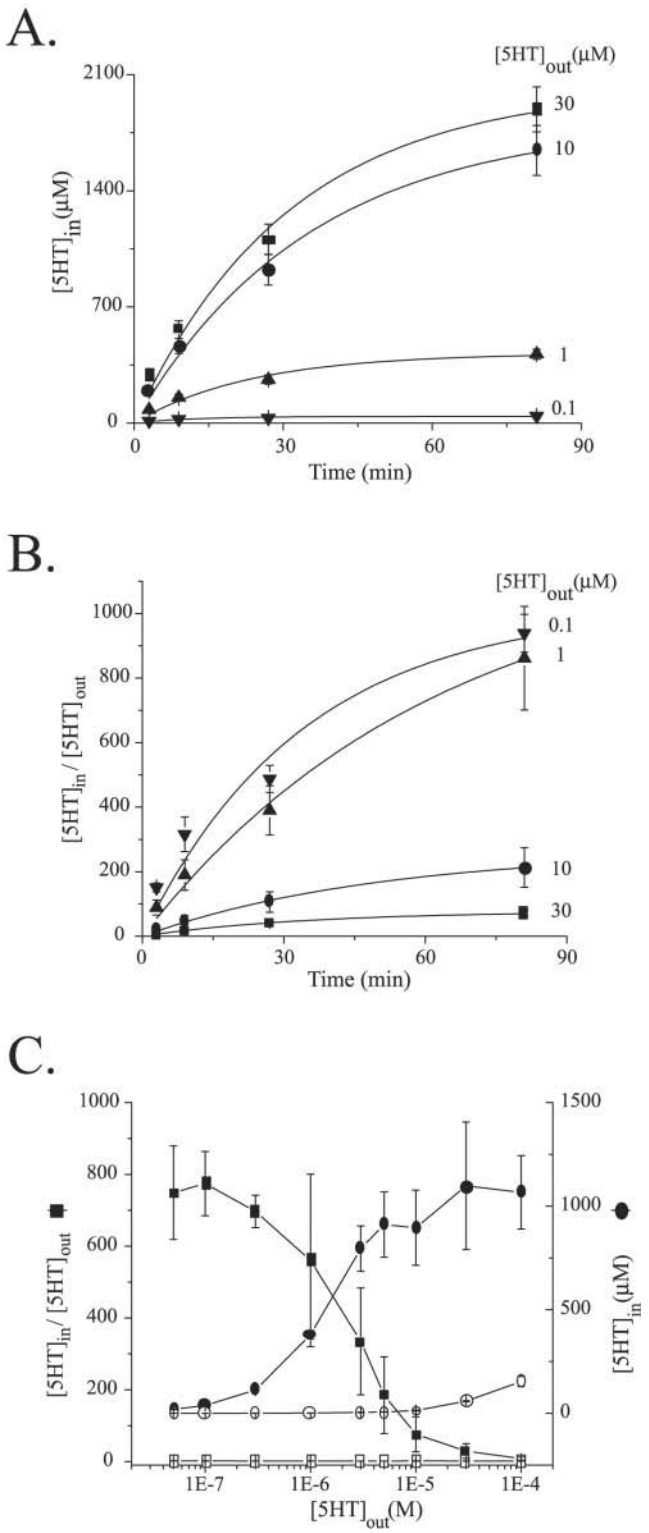

FIGURE 2 HEK-hSERT cells take up 5HT, and establish a 5HT gradient, in a dose- and time-dependent manner. (*A*) Cells were incubated in the indicated $[5HT]_{out}$ for different times (3, 9, 27, or 81 min) and $[5HT]_{in}$ measured with radiolabeled 5HT. (*B*) The 5HT electrochemical gradient, calculated from the data of (*A*) as described in the text. At higher $[5HT]_{out}$, the achieved 5HT gradient is reduced. The lines in (*A*) and (*B*) are fits to the data with the arbitrary form $y = A(1 - e^{-t/\tau})$; parameters are listed in Table 1. (*C*) The 5HT gradient, in this case measured after 81 min of transport, decreases as $[5HT]_{out}$ is increased. Open symbols are control experiments with 750 μM citalopram to block transport.

lated during this 1 min approximates the unidirectional influx of 5HT. As in the measurement of net uptake, each experiment consisted of four experimental wells and two citalopram-treated control wells at each indicated time point. Specific uptake was defined as the difference between the citalopram-untreated and -treated wells.

Efflux transacceleration experiments

Cells were preloaded in KRH with 30 μM 5HT, including 10 nM [^{3}H]-5HT, for 81 min. At this time, the buffer was removed and the cells washed twice with 250 μl ice-cold KRH. To begin the efflux phase of the experiment, 475 μl gKRH buffer was added back to each well, at 22°C, and 25 μl cocktail containing only unlabeled 5HT was added, to bring the final $[5HT]_{out}$ to the indicated concentration. Cells were allowed to efflux for 45 min, then washed twice in 250 μl ice-cold KRH. The labeled 5HT remaining in the cell was counted, and compared to cells loaded with [^{3}H]-5HT but treated with buffer only during the efflux phase.

$[Na]_{in}$ Imaging

HEK-hSERT cells were seeded onto poly-D-lysine-coated glass coverslips and grown for 3 days as above. To facilitate imaging, the cell density was somewhat lower in these experiments than in the uptake experiments. Cell-permeant SBFI-AM (Molecular Probes, Eugene, OR) was dissolved to 10 mM in anhydrous DMSO, and subsequently added to an equal volume of 10% w/v Pluronic F-127 (Molecular Probes). This mixture was diluted into serum-free DMEM so that the final [SBFI-AM] was 2 μM. Before the experiments, the cells were incubated for 90 min at room temperature and protected from light in this media. Upon diffusing across the membrane, SBFI-AM is enzymatically converted into the fluorescent sodium indicator SBFI (Minta and Tsien, 1989). After the dye-loading period, the cells were washed in serum-free DMEM and kept at room temperature, protected from light, until use in an experiment (within 3 h). SBFI is excited at 340 and 380 nm, and fluorescence measured at 500 nm. $[Na]_{in}$ is indicated by the ratio of the excitation at these two wavelengths. Experiments were performed in KRH buffer, supplemented with glucose, as described above. We first measured the $[Na]_{in}$ response to application of 10 μM 5HT. Next, ouabain was added (final concentration 100 μM), in the continued presence of 5HT, and the response measured. Finally, the cells were rinsed with KRH buffer containing 5 μM gramicidin-D several times. The external buffer was then stepped through a series of $[Na]_{out}$ to calibrate the responses previously recorded in the same cells. Although application of gramicidin-D alone may not be sufficient for complete equilibration of $[Na]_{in}$, the calibration procedure at least allows us to determine the sensitivity of the $[Na]_{in}$ measurements. Cells were visualized with a Nikon TE300 inverted microscope (Nikon Instruments Co., Melville, NY). Excitation and emission was measured at the indicated wavelengths with a CCD camera and filterwheel (Sutter Instruments Co., Novato, CA), controlled by a PC. Data was acquired and analyzed using MetaFluor software (Universal Imaging Corp., Downingtown, PA).

Modeling and data analysis

Modeling of the enzymatic transport cycle was done analytically. However, to model the transporter as a single-file pore permeable to two (or more) species, it was necessary to use numerical methods. For the single-file diffusion model, Eq. 13 was solved with the student edition of MatLab

TABLE 1 Parameters from the fits in Fig. 2

$[5HT]_{out}$ (μM)	Internal 5HT		5HT Gradient	
	A (μM)	τ (min)	A	τ (min)
0.1	40 ± 5	12 ± 5	1019 ± 167	34 ± 13
1	420 ± 40	23 ± 6	1184 ± 191	63 ± 18
10	1814 ± 126	35 ± 6	264 ± 22	50 ± 8
30	2024 ± 164	31 ± 6	77.5 ± 6.5	35 ± 7

Data were fit for $[5HT]_{in}$ or $[5HT]_{in}/[5HT]_{out}$ as the y axis to the equation, $y = A(1 - e^{-t/\tau})$.

4 software (The MathWorks, Inc, Natick, MA) running on a standard desktop PC. To solve the necessary differential equation numerically, MatLab uses second- and third-order Runge–Kutta methods.

All experimental data were analyzed with Microcal Origin 6.0 (Microcal Software, Inc, Northhampton, MA) and Excel 2000 (Microsoft Corporation, Richmond, WA) software. Data points represent the average of three ($[5HT]_{out}$ = 30, 3, 1, and 0.1 μM) or twelve ($[5HT]_{out}$ = 10 μM) experiments. Error bars on Figs. 2–5 indicate the standard error of the mean (SEM). To determine the error in the 5HT gradient, the error was propagated in the usual manner. To determine the SEM of the unidirectional flux ratio, only the error in the measurement of the unidirectional influx was propagated. Error in the derivative of the fit used to determine net velocity was neglected. Fits were performed with the Origin software, which uses a Levenberg–Marquardt algorithm. The errors were not used to weight the data points for fitting.

RESULTS

Uptake time course

Figure 2 *A* shows that HEK-hSERT cells exposed to 5HT immediately begin to take it up. After only 3 min, cells in 10 μM external 5HT have already loaded approximately 100 pmole of 5HT/well, yielding $[5HT]_{in}$ = 160 μM. As time progresses, the amount of 5HT inside the cells increases, and the net uptake velocity (slope of the fitted curves) decreases. The data were fit to the exponential function $y = A(1 - e^{-t/\tau})$, where y is the net uptake. Other choices are possible, e.g., allowing an offset at $t = 0$ or using the similarly shaped hyperbolic function $y = At/(\tau + t)$, and these cases were examined. Allowing an offset at $t = 0$ did not significantly change the values of A or τ, for either the exponential or hyperbolic expression. Using the hyperbolic function rather than the exponential function yielded similar values of τ but higher values of A. The ranges of uncertainty in the fit parameters generated with either function overlapped. We emphasize, however, that the choice of fitting function, $A(1 - e^{-t/\tau})$ is arbitrary, and that none of the qualitative conclusions drawn from its use depend on this choice. The parameters from the fits are given in Table 1.

For increasing $[5HT]_{out}$, the expectation is that, at equilibrium, more 5HT will be inside the cells. The ionic gradients that SERT uses to establish a 5HT gradient are constant (see Fig. 6), and raising $[5HT]_{out}$ should result in a proportional increase in $[5HT]_{in}$. Thus, in changing $[5HT]_{out}$ from 0.1 to 1.0 μM, a 10-fold increase in $[5HT]_{in}$ is expected and realized. However, increasing $[5HT]_{out}$ from 1 to 10 μM, only a four-fold increase in $[5HT]_{in}$ is measured (Table 1).

In Fig. 2 *B*, the 5HT gradient across the membrane, $[5HT]_{in}/[5HT]_{out}$ is plotted over time. To calculate the gradient from the data in Fig. 2 *A*, we assumed that, as 5HT accumulates in the cells, the [5HT] decreases in the bath,

$$[5HT]_{out} = [5HT]'_{out} - 5HT_{in}/V, \tag{19}$$

where $5HT_{in}$ is the amount of 5HT accumulated in the cells (pmole), $[5HT]'_{out}$ is the initial $[5HT]_{out}$, and V is the volume of the bath (500 μl). Thus, the calculated 5HT gradient plotted in Fig. 2 *B* is determined according to

$$\frac{[5HT]_{in}}{[5HT]_{out}} = \frac{5HT_{in}/(NV_{cell})}{[5HT]'_{out} - 5HT_{in}/V}, \tag{20}$$

where N is the number of cells per well (see Methods) and V_{cell} is the volume of each cell (1.25 pl) (Sitte et al., 2001).

Figure 2 *B* suggests that the established [5HT] gradient decreases as $[5HT]_{out}$ increases. This is further illustrated in Fig. 2 *B*. The 5HT gradient, measured following 81 min of uptake, is constant for $[5HT]_{out}$ below ~1 μM, but decreases as $[5HT]_{out}$ increases beyond 1 μM. Figure 2 *C* also shows that the total $[5HT]_{in}$ is still increasing at $[5HT]_{out}$ doses up to 3 μM, even as the gradient $[5HT]_{in}/[5HT]_{out}$ is decreasing. Thus, the observed decrease in the gradient at high $[5HT]_{out}$ compared to low $[5HT]_{out}$ is not due only to saturation of $[5HT]_{in}$.

Unidirectional influx

Figure 3*A* displays the measured values of the unidirectional influx for cells preloaded with initial $[5HT]_{out}$ of 30, 10, 1, and 0.1 μM. The x axis indicates the time for which the cells were preloaded at the indicated concentration. Measurement of the unidirectional influx began at this time and lasted one minute, as described in the Methods. To calculate the unidirectional influx from the measured [^{3}H]-5HT influx, two assumptions are necessary. First, we assumed that the measured [^{3}H]-5HT influx during one minute represents the actual unidirectional influx, not net flux. Second, $[5HT]_{out}$ must be known, so that unidirectional influx is measured by [^{3}H]-5HT accumulation. Again we assumed that the total 5HT was constant, and therefore the external concentration decreased as $[5HT]_{in}$ increased during the loading phase, according to Eq. 19. We also took into account the increase in the $[5HT]_{out}$ due to the addition of the challenge cocktail used to measure the unidirectional influx. With these corrections, the values for unidirectional influx of 5HT are shown in Fig. 3 *A*.

For comparison, the net flux was calculated from Fig. 2 *A* and plotted as a line in Fig. 3 *A* for each $[5HT]_{out}$. At all times, the unidirectional influx is greater than or equal to the net influx, as must be the case. Although the net influx and unidirectional influx should be the same at $t = 0$, our

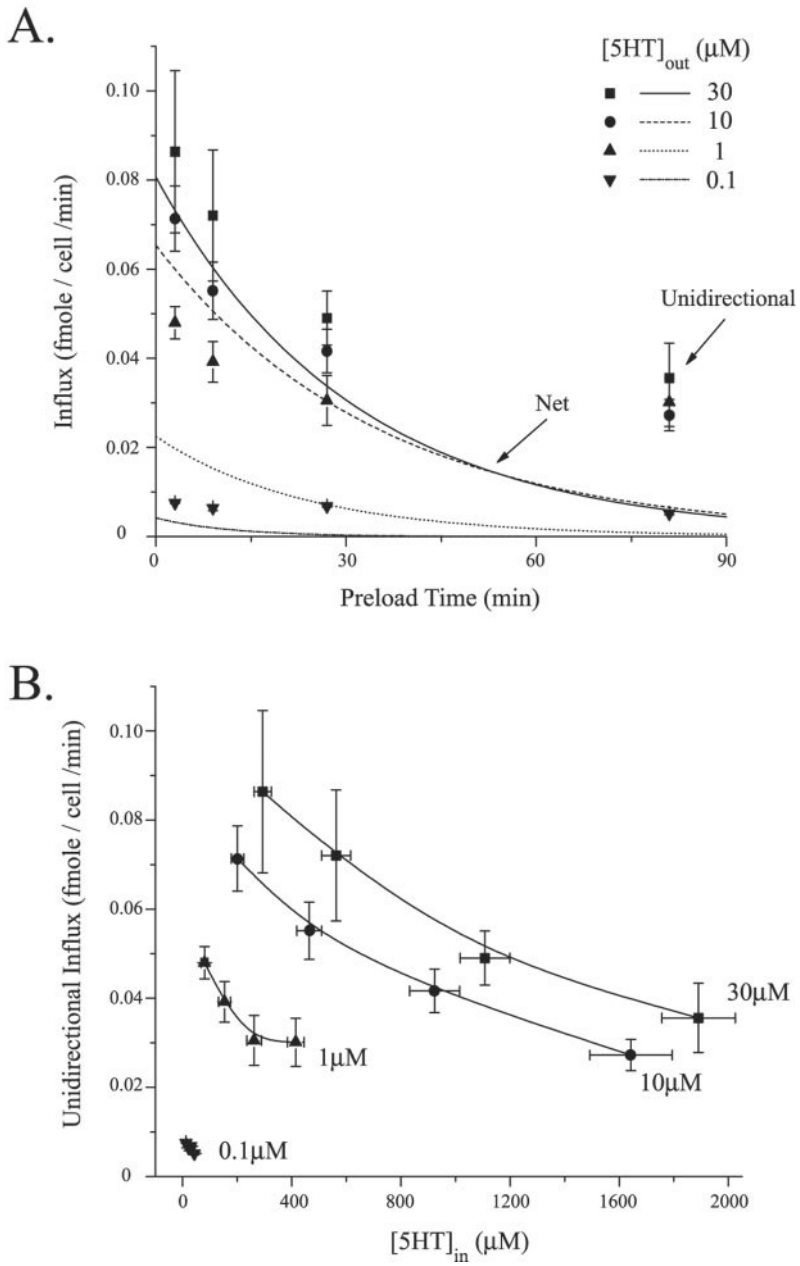

FIGURE 3 Measurement of the unidirectional influx of 5HT. (*A*) HEK-hSERT cells preloaded for the indicated time in unlabeled 5HT at 30 μM (*squares*), 10 μM (*circles*), 1 μM (*upward triangles*), or 0.1 μM (*downward triangles*) and challenged for one minute with radiolabeled 5HT. Lines represent the net flux, as determined by taking the time derivative of the fits to the data of Fig. 2 *A*. (*B*) Unidirectional influx decreases with internal 5HT. Unidirectional influx data are taken from (*A*), and internal 5HT from Fig. 2 *A*. The data were correlated by time point and plotted against one another.

measurements deviate from this expectation. One possibility is that the measurement of the net uptake velocity, Fig. 2 *A*, misses a fast component of uptake, because the shortest incubation time was 3′. This causes the measurement of the net velocity to be an underestimate of the true value at earlier times. We have not compensated for this possibility, because it does not affect our conclusions. Figure 3 recasts the data of Figs. 2 *A* and 3 *A*, by plotting, for each time point and each $[5HT]_{out}$ condition, the value of the unidirectional influx against the internal 5HT. As the cells accumulate internal 5HT, both net and unidirectional influx decrease.

Efflux transacceleration

Figure 4 examines the efflux of 5HT from cells preloaded with labeled 5HT. Cells were loaded at 30 μM 5HT for 81 min and allowed to efflux for 45 min at the tested $[5HT]_{out}$. The data are expressed as the amount of 5HT effluxed during this 45 min, as a percentage of the 5HT remaining in cells that were identically loaded but subsequently exposed only to buffer. A hyperbolic fit to the data yields a maximal efflux of 62 $\pm$ 3% with a K_m = 6.3 $\pm$ 0.8 μM. Thus, as $[5HT]_{out}$ increases, the efflux of internal 5HT increases. This phenomenon is referred to as "transacceleration," and is often interpreted as evidence of a classical transport mechanism (Stein, 1986 pp 240–241).

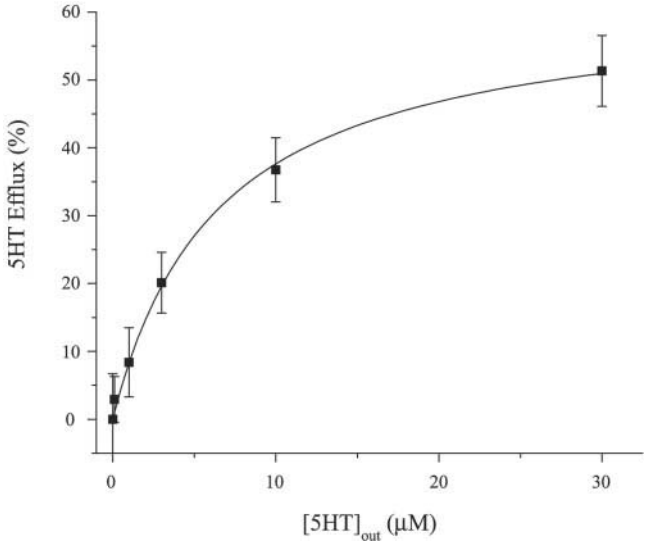

FIGURE 4 Efflux is transaccelerated. HEK-hSERT cells were preloaded for 81 min in 30 μM 5HT containing [^{3}H]-5HT, then washed and exposed for 45 min to a single concentration of unlabeled 5HT. The line represents a fit to a hyperbola.

Unidirectional flux ratio

By measuring the net flux and the unidirectional influx in identically treated cells, we can construct the ratio of the unidirectional efflux to the unidirectional influx,

$$\frac{\phi_{out}}{\phi_{in}} = 1 - \frac{\Phi}{\phi_{in}}. \quad (21)$$

Here ϕ_{out} and ϕ_{in} are the unidirectional efflux and influx, and Φ is the net flux. Hence the right-hand side of Eq. 21 represents the measured quantities. Figure 5 plots the unidirectional flux ratio against the internal 5HT determined from Fig. 2 *A* for each time. The data at 0.1 and 1 μM fit straight lines $y = Ax + B$ (0.1 μM: $A = (1.49 \pm 0.33) \times 10^{-2}$ μM^{-1}, $B = 0.4 \pm 0.1$; 1 μM: $A = (1.22 \pm 0.14) \times 10^{-3}$ μM^{-1}, $B = 0.46 \pm 0.04$). The intercepts of the data are not zero, due to offset errors in the unidirectional and net fluxes, as discussed previously. At higher $[5HT]_{out}$, we fit the combined data from $[5HT]_{out} = 10$ and 30 μM to a quadratic polynomial, of the form $y = A + Bx + Cx^2$, where y is the flux ratio and x is $[5HT]_{in}$. The parameters were $A = 0.150 \pm 0.064$, $B = (-1.42 \pm 1.59) \times 10^{-4}$ μM^{-1}, and $C = (2.81 \pm 0.75) \times 10^{-7}$ μM^{-2}.

Control experiments

In some experiments, the fractional decrease in $[5HT]_{out}$ is as much as 50% and must be taken into account when the data are analyzed, as described by Eqs. 19 and 20. This correction technique has an experimental advantage because the cells achieve equilibrium more quickly, reducing the time that the cells remain under potentially stressful experimental conditions. However, as a control against unknown errors due to consumption of the external 5HT, uptake time course experiments were performed on HEK-hSERT cells plated at a lower density to reduce consumption of $5HT_{out}$. For these experiments, cells were seeded on poly-D-lysine-coated plates at 10^3 cells/well and allowed to grow under standard conditions for one day. One experiment was performed in a 24-well plate, with $[5HT]_{out} = 10$ or 1 μM. The second experiment was performed in a 48-well plate, with $[5HT]_{out} = 10$, 5, 1, or 0.1 μM. Other experimental details

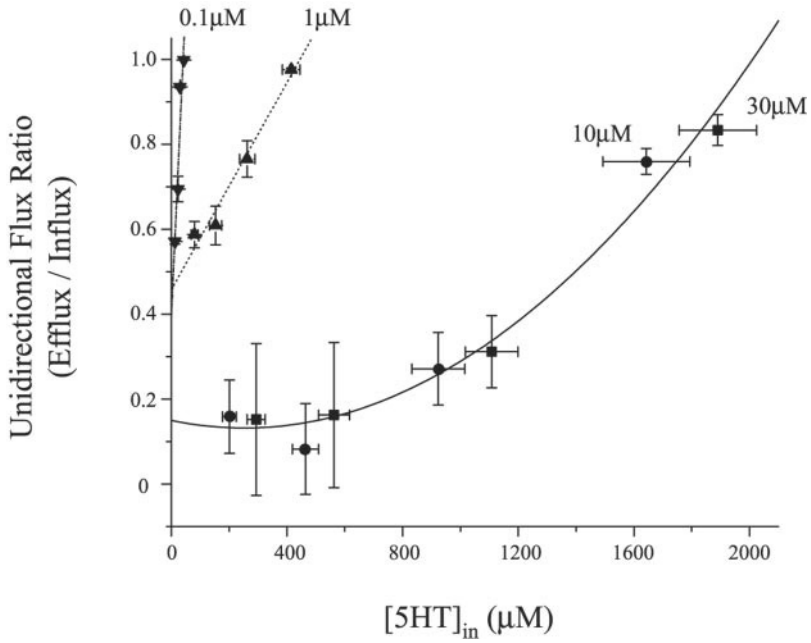

FIGURE 5 The unidirectional flux ratio as a function of $[5HT]_{in}$. The values of $[5HT]_{in}$ were taken from Fig. 2 *A*. The lines at 0.1 and 1 μM are linear fits to the data points. The data at 10 and 30 μM were pooled and fit to a quadratic equation, as shown. Thus, at higher $[5HT]_{in}$, resulting from higher $[5HT]_{out}$, the nonlinear dependence of the flux ratio is revealed.

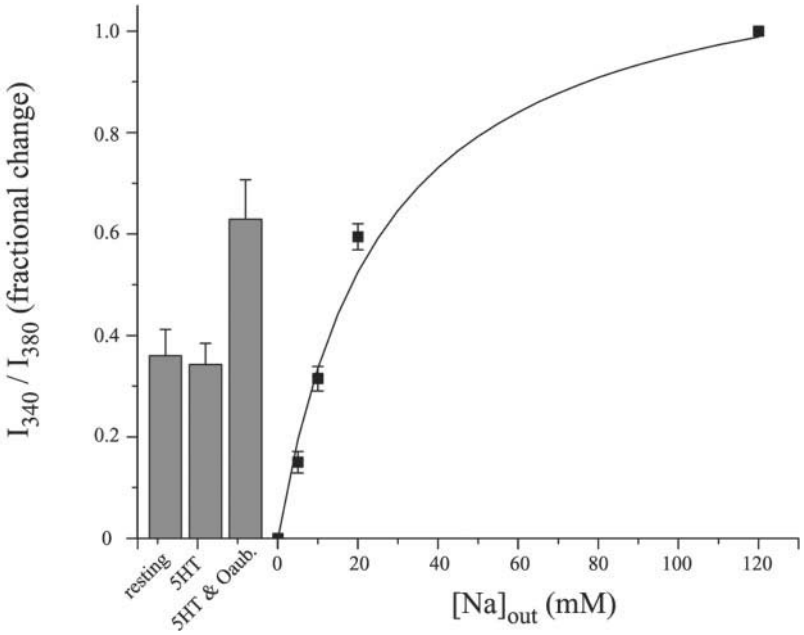

FIGURE 6 Measurement of $[Na]_{in}$. The application of $[5HT]_{out}$ = 10 μM does not change $[Na]_{in}$ appreciably, compared to untreated cells, when the Na/K-ATPase is functional. Disruption of the Na/K-ATPase in the presence of 5HT induces an increase in $[Na]_{in}$ (*bars*). The calibration curve was obtained by changing $[Na]_{out}$ after permeablizing cells with application of 5 μM gramicidin-D.

were identical to the uptake time course experiments described above. We could not measure the unidirectional flux at low cell density because the [^{3}H]-5HT signal was too small. We also noted that low cell density resulted in a high fractional loss of cells during the repeated washing. However, the primary results were the same as in the experiments at high cell density. Explicitly, the equilibrium 5HT gradient was smaller for cells incubated in 10 μM $[5HT]_{out}$ compared with cells incubated at 1 μM.

In addition to plating cells at lower densities, we also sampled the incubation bath during one experiment on the high-density HEK-hSERT cells. This experiment is included in the data of Figs. 2 and 3, performed at 10 and 0.1 μM initial $[5HT]_{out}$. A 5-μl sample was taken from three wells (two experimental and one citalopram-controlled well) after 81 min of uptake, for each initial $[5HT]_{out}$. The bath sample was added to a scintillation vial containing 500 μl 1% SDS and 3 mL scintillation fluid, and counted as described in Methods. The measured $[5HT]_{out}$ agreed with our calculated $[5HT]_{out}$ to within 3 and 10% for 10 and 0.1 μM $[5HT]_{out}$, respectively. This result supports our 5HT gradient correction procedure, Eq. 19 and Eq. 20, and implies that a small fraction of cells was lost during repeated washing, when cells are plated and grown at high density. Note that, at 0.1 μM, the signal (cpm) given by a 5-μl aliquot of the bath is small, and low signal-to-noise ratio elevates the apparent measured $[5HT]_{out}$. From the net uptake time course (Fig. 2), we infer that, during the loading phase, cells can transport enough 5HT to reduce $[5HT]_{out}$ by as much as 50%. The reduction in unidirectional influx is due in part to this depletion. However, for the experiments at $[5HT]_{out}$ = 30 and 10 μM, depletion of $[5HT]_{out}$ is small (10%), but the unidirectional influx is still observed to decrease with increasing $[5HT]_{in}$.

We also measured changes in $[Na]_{in}$ caused by the application of 10 μM 5HT, to test our assumption that the sodium gradient is not changed during the course of our uptake experiments (Fig. 6). In the absence of external ouabain, we could not detect a significant change in $[Na]_{in}$ due to stimulation with 5HT, over a 20-min experiment. When ouabain was added, we observed an immediate increase in $[Na]_{in}$ from the tonic level. These data indicate that application of 5HT does not decrease the sodium gradient in cells with functioning Na/K-ATPase proteins.

Finally, to explain the drop in the 5HT gradient, we address the possibility of flux pathways, other than hSERT, for 5HT into and out of the stably transfected cells. Recent literature indicates that some alternate pathways may exist, when the hSERT protein is blocked by high levels of a specific inhibitor (Scholze et al., 2001; Sitte et al., 2000). To examine this possibility, we repeated some of the experiments of Scholze et al. (2001) in our system. HEK-hSERT cells were exposed to 10 μM 5HT for 9 or 81 min, exactly as described for the time course experiments above. However, after accumulating 5HT, the cells were then washed twice in buffer without 5HT, but containing 100 μM citalopram. We then assayed efflux by measuring the 5HT remaining in the cells after 5 min of efflux, and compared this with cells whose 5HT content was measured immediately after washing with citalopram. This "load-and-block" experiment is expected to reveal nonspecific (i.e., other than

hSERT) efflux pathways through the HEK–hSERT cell membrane, because any escaping 5HT cannot be transported back into the cell via hSERT. We found that the rate of nonspecific 5HT efflux was 0.066 ± 0.022 fmole/cell/min for cells loaded with 5HT for 81 min, or 0.0044 ± 0.0075 fmole/cell/min for cells loaded for 9 min (3 experiments, 4 wells/experiment). The first of these measurements agrees reasonably with the published data (Scholze et al., 2001) for these cells; although our protocols differ somewhat, we note that $[5HT]_{in}$ levels are similar.

To further characterize this nonspecific pathway, two uptake time course experiments were performed on parental HEK-293 cells at $[5HT]_{out} = 10$ or 1 μM. No significant difference was observed between cells treated with 100 μM citalopram and untreated cells, and the total uptake was less than 5% of uptake in identically tested hSERT transfected cells. Thus, in HEK-hSERT cells exposed to micromolar $[5HT]_{out}$, the predominant pathway for 5HT into the cell is the hSERT protein. However, at high $[5HT]_{in}$, nonspecific pathways may contribute to depletion of the 5HT gradient, and confound measurements of the flux ratio.

DISCUSSION

5HT Gradients

Figure 2 demonstrates that HEK-hSERT cells effectively transport external 5HT into their interior in a time- and dose-dependent manner. Thus the initial rate of transport is observed to increase with increasing $[5HT]_{out}$. However, as time progresses, the cells accumulate 5HT, and this leads to a slowing of net transport. After a sufficiently long time, $[5HT]_{in}$ reaches a level many times higher than $[5HT]_{out}$, as illustrated in Fig. 2 *B*. At this point, hSERT is no longer able to increase $[5HT]_{in}$, and the transport process has reached equilibrium. For each 5HT molecule transported into the cell, a 5HT molecule must, on average, leave the cell; unidirectional influx and efflux are balanced. Both models share this same qualitative behavior.

Figure 2 *B* displays a quantitative failure of the enzymatic model, which is further examined in Fig. 2 *C*. Comparison of the 5HT gradient between the experiments reveals that, as $[5HT]_{out}$ increases, the ability of hSERT to maintain a 5HT gradient decreases. Thermodynamic analysis of a strict stoichiometric coupling process, as in the enzymatic model, predicts that the substrate gradient (ratio of concentrations) is independent of substrate concentrations (absolute values). Our data contradict this theoretical result, suggesting that an underlying assumption of the enzymatic model, viz., stoichiometric coupled transport, is incorrect.

One way to recover the enzymatic model would assume fixed stoichiometry at fixed $[5HT]_{out}$, but that stoichiometric ratio m decreases with increasing $[5HT]_{out}$ due to low-affinity binding sites on hSERT. An alternative explanation is that the coupling ratio is never fixed at any concentration, as in the single-file pore, with n sites occupied by either sodium or 5HT. One sees naturally that, as 5HT occupies more sites in elevated $[5HT]_{out}$, the average coupling ratio is lowered. The average ratio of sodium-occupied sites to 5HT-occupied sites governs coupling and results in the dependence seen in Fig. 2.

To further test the possibility of single-file coupling, we compare our data to a numerical simulation of a single-file pore permeable to 5HT and sodium (Fig. 7). Transport of 5HT and sodium through an idealized single-file pore obeys the differential Eq. 13. The units of [Na] and [5HT] in Eq. 13 are arbitrary, in the sense that these effective concentrations contain unknown permeability factors. Therefore, the magnitudes of these terms were chosen arbitrarily, but the ratios of the values correspond to the ratios of the experimental values. In these numerical calculations, we fix the number of pore sites to $n = 3$, $[Na]_{out} = 120 \times 10^3$, $[Na]_{in} = 12 \times 10^3$, and $[5HT]_{out} = 10$, 1, or 0.1 but allow $[5HT]_{in}$ to change freely as 5HT is transported.

The results of the numerical solution to Eq. 13 (channel model) are displayed in Fig. 7 *A*. As expected from the intuitive argument above, $[Na]_{out} \gg [5HT]_{out}$ produces a robust 5HT gradient. If, in addition, $[Na]_{in} \gg [5HT]_{in}$, the channel model can achieve a gradient equal to the thermodynamic limit (Eq. 1)

$$\frac{[5HT]_{in}}{[5HT]_{out}} = \left(\frac{[Na]_{out}}{[Na]_{in}}\right)^{n}, \tag{22}$$

which is identical to the ideal enzymatic model with n (pore length) playing the role of m (stoichiometry). Thus, for $n = 3$ in the channel model, the 5HT gradient approaches 1000 at low $[5HT]_{out}$. However, in the channel model, but not in the enzymatic model, the 5HT gradient decreases as $[5HT]_{out}$ increases in accord with the data in Fig. 2 *B*.

Finally, we considered the possibility that the collapse of the 5HT gradient at high $[5HT]_{out}$ is an artifact, produced by the nonspecific efflux of 5HT from the cells. Nonspecific efflux has been documented for these cells (Scholze et al., 2001), and we also measured a significant maximal nonspecific rate of efflux (0.066 ± 0.022 fmole/cell/min) similar to the published results. To estimate the impact of this efflux on our results, we assume that, in the absence of nonspecific efflux, hSERT would maintain a high 5HT gradient regardless of $[5HT]_{out}$. We can test, therefore, whether the difference between the observed gradients at $[5HT]_{out} = 0.1$ μM and $[5HT]_{out} = 30$ μM is due to nonspecific efflux, and calculate the amount of 5HT that must have escaped through this pathway over the course of our experiment. The 5HT gradients after 81 min of transport were 858 and 70 at $[5HT]_{out} = 0.1$ μM and $[5HT]_{out} = 30$ μM, respectively (Fig. 2). These gradient values take into account the depletion of the external substrate, as discussed previously (Eqs. 19 and 20), and here we also take into account this restriction. Had the $[5HT]_{out} = 30$ μM experiment achieved the

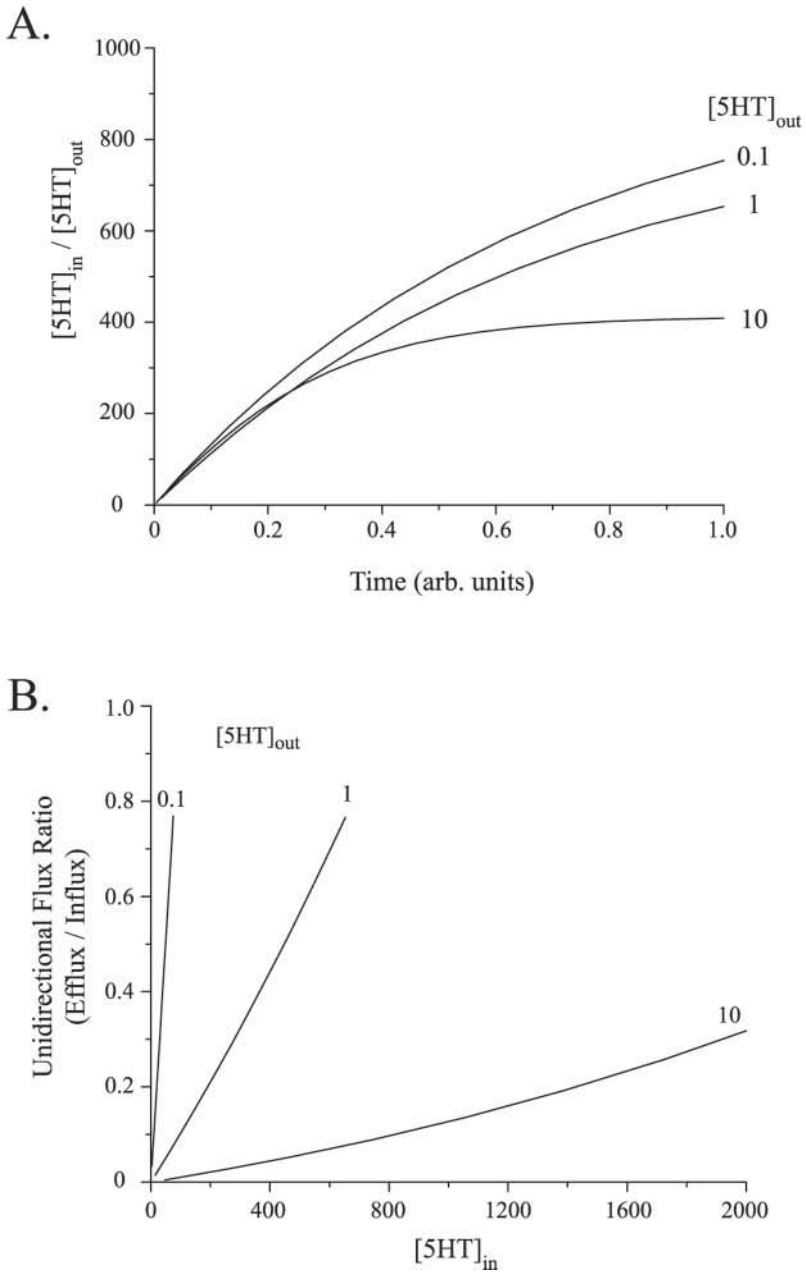

FIGURE 7 Predictions of the 5HT gradient and unidirectional flux ratio produced by hSERT functioning as a single-file pore, permeable to 5HT and sodium, with $n = 3$ sites. The lines are the numerical solution to Eq. 5, assuming $[Na]_{out} = 120 \times 10^3$, $[Na]_{in} = 12 \times 10^3$, and $[5HT]_{out}$ as indicated. (*A*) As $[5HT]_{out}$ increases, a lower 5HT gradient is produced. Compare to Fig. 2. (*B*) At low $[5HT]_{out}$, the flux ratio is a linear function of the 5HT gradient whose slope is inversely proportional to $[5HT]_{out}$. At higher $[5HT]_{out}$, this is not the case. Compare to Fig. 5.

same gradient as the $[5HT]_{out} = 0.1$ μM experiment, the external bath would have been depleted to ~14.5 μM, and the $[5HT]_{in}$ would have been ~12.4 mM. However, the measured value was 1.89 mM; hence, ~10.5 mM are missing. Assuming the cell volume ~1.25 pl, this represents ~13.1 fmole 5HT, which escaped over an 81-min experiment. Hence the average nonspecific leak pathway, which worked to destroy the achievable 5HT gradient, was 13.1 fmole/81 min = 0.16 fmole/min/cell.

Because the nonspecific efflux was measured in cells over 5 min, this measured nonspecific efflux (0.066 ± 0.0022 fmole/cell/min) represents the maximal nonspecific efflux. This nonspecific efflux cannot account for the depletion of the gradient, because to explain our results (Fig. 2) would require that the average nonspecific efflux over the entire 81-min experiment exceed the maximal efflux rate experimentally determined. Thus, the measured nonspecific efflux is insufficient to explain the observed depletion of the 5HT gradient. Our results most likely reveal an inherent property of hSERT; namely, imperfect coupling.

Unidirectional flux

Although Fig. 2 *A* shows how net 5HT flux changes as cells load 5HT, without explicit measurement it is not apparent

why the unidirectional flux ratio changes. One possibility is that unidirectional influx is constant for fixed $[5HT]_{out}$, but unidirectional efflux increases with $[5HT]_{in}$. Also possible is that unidirectional influx increases with internal 5HT, as predicted by transacceleration, provided that influx minus efflux produces the net transport in Fig. 2 *A*. Contrary to the enzymatic model, which envisages *trans* 5HT to accelerate flux (Stein, 1986, pp 240), unidirectional influx actually decreases as $[5HT]_{in}$ increases (Fig. 3). The single-file channel model offers a straightforward explanation of Fig. 3, because internal 5HT would impede 5HT influx.

In contrast, Fig. 4 reveals an apparent transacceleration in the outward direction. Cells were preloaded with 30 μM 5HT, a fraction of which was labeled, for 81 min, analogous to the last time points in Fig. 2. After loading, cells were exposed to external 5HT for 45 min to measure net efflux of [^{3}H]-5HT. We observed that the efflux of labeled 5HT increased with increasing external 5HT, as reported previously for SERTs (Nelson and Rudnick, 1979; Sitte et al., 2000, 2001). The transacceleration seen in Fig. 4 is taken as evidence for an enzymatic mechanism and against a channel mechanism (Stein, 1986, pp 241). In the enzymatic interpretation, *trans* substrate allows transporters to avoid the slow return of the empty transporter; thus external 5HT import would accelerate internal 5HT export. A channel, it is argued, would be blocked by *trans* substrate. However, Fig. 4 is net flux, not unidirectional flux, and does not rule out a channel mechanism if external 5HT opens channels. Whereas both models can display transacceleration, as reported in Fig. 4, only the channel model evidently describes the unidirectional flux experiment in Fig. 3.

Unidirectional flux ratio

To find an analytical parameter describing the mechanism of coupled transport, we considered ways to eliminate gating phenomena and focus on permeation. By constructing the ratio of the unidirectional fluxes, we eliminate processes necessary for permeation in both directions. Hence, the effect of gates on one or both ends of the pore will be divided out of the flux ratio. As discussed in the Theory section, we expect that, under some conditions, the flux ratio may distinguish between coupling mechanisms.

With this in mind, consider Fig. 5, where the unidirectional flux ratio is plotted as a function of $[5HT]_{in}$. For $[5HT]_{out} = 0.1$ and 1 μM, ϕ_{out}/ϕ_{in} increases linearly with accumulating $[5HT]_{in}$. However, as the $[5HT]_{out}$ is increased to 10 μM, the power-law dependence on $[5HT]_{in}$ becomes evident, as predicted from the channel model (Eq. 14). As $[5HT]_{out}$ is further increased to 30 μM, no change in the flux ratio is observed, because the values of $[5HT]_{in}$ are comparable in 10 and 30 μM 5HT. The difference between flux ratios below 1 μM and above 10 μM external 5HT result from internal 5HT failing to accumulate proportional to external 5HT, which is unexpected in the enzymatic model but predicted in the channel model.

We used numerical simulations of the single-file pore model to compare with the data. The results are shown in Fig. 7 *B*, where model parameters were as described above in 5HT gradients. The channel model predicts that the slope of the flux ratio as a function of $[5HT]_{in}$ depends inversely on $[5HT]_{out}$ (Eq. 14). In contrast, the enzymatic model predicts that the slope is approximately independent of $[5HT]_{out}$ (Eq. 9). The latter conclusion depends, however, on the value of K in the enzymatic model. Thus, although the flux ratio is immediately consistent with the channel model, appropriate rate constants may recover the enzymatic model.

The channel model also predicts a quantitative relation between the flux ratio as a function of the $[5HT]_{in}$ (Fig. 5) and the failure of hSERT to achieve high 5HT gradients as $[5HT]_{out}$ increases (Fig. 2). Assume that $[Na]_{out} \gg [5HT]_{out}$ and rearrange Eq. 14 to

$$\frac{\phi_{out}}{\phi_{in}} = \frac{[5HT]_{in}}{[5HT]_{out}} \left(\frac{[Na]_{in}}{[Na]_{out}}\right)^n \left(1 + \frac{[5HT]_{in}}{[Na]_{in}}\right)^n, \quad (23)$$

and the expression for the equilibrium 5HT gradient Eq. 15 to

$$\frac{[5HT]_{in}}{[5HT]_{out}} = \left(\frac{[Na]_{out}}{[Na]_{in}}\right)^n \left(\frac{1}{1 + [5HT]_{in}/[Na]_{in}}\right)^n. \quad (24)$$

Because the same factor $(1 + [5HT]_{in}/[Na]_{in})^n$ appears in each expression, we expect that the failure of the [5HT] gradient predicted by Eq. 24 will be inversely related to the relation between the flux ratio slopes in Eq. 23. Examination of the data shows that we observed a five-fold decrease in the [5HT] gradient between 1 and 10 μM $[5HT]_{out}$. Hence, the final factor in Eq. 24 equals 5. Therefore, the final factor in Eq. 23 should be ⅕. Consistent with this, we observed that, when the flux ratio at 1 μM was only two- to three-fold, rather than ten-fold, larger than the slope at 10 μM $[5HT]_{out}$. Therefore, our observations are internally consistent with the single-file pore model.

To reiterate our findings, Fig. 2 shows that hSERT establishes a higher 5HT gradient at low $[5HT]_{out}$ than at high $[5HT]_{out}$. In addition, the ratio of the unidirectional fluxes permeating hSERT depends on $[5HT]_{out}$, has a nonlinear dependence on $[5HT]_{in}$, and does not saturate up to $[5HT]_{in} = 2$ mM (Fig. 5). A single-file pore model of co-permeation for 5HT and sodium directly predicts these results (Fig. 7). In contrast, a simple enzymatic cycle of stoichiometric 5HT and sodium transport is contradicted by the failure of the 5HT gradient in high $[5HT]_{out}$. More complex enzymatic models, which allow for the uncoupled transport of 5HT, also fail because they predict a lower 5HT gradient, independent of $[5HT]_{out}$, for a given set of ionic conditions (Stein, 1986). Finally, because we have measured only the

flux of 5HT, the addition of an uncoupled sodium channel that is impermeable to 5HT does not change our conclusion that the enzymatic model of 5HT transport is insufficient to explain our data.

Although we know little about the three-dimensional (3D) structure of sodium-coupled transporters, the 3D structure of the H-coupled oxalate transporter, OxlT (Hirai et al., 2002) is now available. At 6.5-Å resolution, the structure reveals 12 helices that form a transmembrane pore with a wide central cavity. Four helices face the channel throughout their length, and four others line the channel on one or the other side. Whereas enzymatic models invoke two conformations in which a substrate-binding site is alternately accessible to one or the other side, Hirai et al. (2002) envisage a symmetric conformation that has comparable accessibility to both external and internal sides of the membrane. Though the structure is consistent with a channel model, these images represent average configurations from which it is difficult to infer mechanisms.

One might consider that transport of sodium and chlorine ions would be unlikely in a pore. Indeed, there are no examples of ion channels that selectively carry both cations and anions. Although evidence for thermodynamically coupled, selective cotransport is clear-cut for sodium, no similar evidence exists for chlorine for serotonin transporters, which retain 20% uptake and 40% induced current with acetate replacing chlorine (Galli et al., 1997). Indeed, in SERT at least, chlorine ions may be regulatory rather than cotransported (Lin et al., 1996). Finally, serotonin influx is reportedly coupled to potassium-or hydrogen-ion efflux (Nelson and Rudnick, 1979; Gu et al., 1996), which might be thought to present difficulties to single-file permeation. It is well known, however, that potassium ions influx and efflux single-file through the same pore, albeit not simultaneously, and that potassium flux is coupled to itself (Hodgkin and Keynes, 1955). A similar concept has been expounded for entropy-driven pumps (Chou and Lohse, 1999). Thus bi-direction flux presents no obstacle to the single-file channel model.

Our findings support the idea that 5HT permeates hSERT through a channel, as previously demonstrated at high $[5HT]_{out}$ for the *Drosophila* SERT (Galli et al., 1997; Petersen and DeFelice, 1999) and the human norepinephrine transporter (Galli et al., 1996, 1998). Our results suggest that 5HT permeates not only at high $[5HT]_{out}$ but virtually all concentrations, because we observe departure from the stoichiometric model for $[5HT]_{out}$ as low as 3 μM (Fig. 2 *C*). It is possible that hSERT switches between strict stoichiometric coupling below 3 μM and nonfixed, partially uncoupled permeation above this value. However, we consider this unlikely. We propose instead that coupling occurs in a narrow pore, permeable to sodium, other coupled ions, and 5HT, and that coupling depends on chance biased by the absolute concentrations of the permeating species. This model views coupling not as a fixed parameter but rather as an average property of copermeation that accounts for both concentrative uptake and electrophysiological data.

Indeed, in some previous work, the enzymatic cycle model has been represented as a "pore" with gates on both ends (Cao et al., 1998). Such a model assumes that, during coupled 5HT transport, the gates are not simultaneously open, and that a stoichiometric binding triggers the appropriate gating. We point out, however, that the assumption of synchronized gating is unnecessary to preserve coupled transport. Rather, coupling is preserved in the microscopic conditions of synaptic transmission, namely, high $[Na]_{out}$ and comparatively low $[5HT]_{out}$. Immediately following exocytotic release of neurotransmitter such as 5HT, $[5HT]_{out}$ may reach millimolar values (Bunin and Wightman, 1998). Under this condition the transporter merely need function as a pore, because the 5HT gradient drives 5HT transport into the cell. Indeed, a pore mechanism may produce a higher instantaneous clearance rate than an enzymatic mechanism. As $[5HT]_{out}$ declines, coupling to the ionic gradients would be necessary to continue 5HT transport against the local high $[5HT]_{in}$ as may exist at the internal face of the membrane. We have shown that a narrow pore efficiently couples ionic gradients to [5HT] gradients at low $[5HT]_{out}$. Thus, a single-file channel mechanism of cotransport is well suited to the dynamic environment of synaptic transmission and clearance.

The authors thank Dr. Randy Blakely for supplying HEK-hSERT cells and thoughtful discussion; Dr. Kevin Strange and Dr. Eric Rutledge for use of equipment and technical assistance with [Na] imaging; and Hongping Yuan for excellent tissue culture.

This work was supported by National Institutes of Health grant NS-34075.

REFERENCES

Blakely, R. D., H. E. Berson, R. T. Fremeau, Jr., M. G. Caron, M. M. Peek, H. K. Prince, and C. C. Bradley. 1991. Cloning and expression of a functional serotonin transporter from rat brain. *Nature.* 354:66–70.

Blakely, R. D., L. J. DeFelice, and H. C. Hartzell. 1994. Molecular physiology of norepinephrine and serotonin transporters. *J. Exp. Biol.* 196:263–281.

Bunin, M. A., and R. M. Wightman. 1998. Quantitative evaluation of 5-hydroxytryptamine (serotonin) neuronal release and uptake: an investigation of extrasynaptic transmission. *J. Neurosci.* 18:4854–4860.

Cao, Y., M. Li, S. Mager, and H. A. Lester. 1998. Amino acid residues that control pH modulation of transport-associated current in mammalian serotonin transporters. *J. Neurosci.* 18:7739–7749.

Chou, T., and D. Lohse. 1999. Entropy-driven pumping in zeolites and biological channels. *Phys. Rev. Lett.* 82:3552–3555.

DeFelice, L. J., and S. V. Adams. 2001. Serotonin and norepinephrine transporters: possible relationship between oligomeric structure and channel modes of conduction. *Mol. Membr. Biol.* 18:45–51.

DeFelice, L. J., S. V. Adams, and D. Ypey. 2001. Single-file diffusion and neurotransmitter transporters: Hodgkin's mechanical model revisited. *BioSystems.* 62:57–66.

Doyle, D. A., C. J. Morais, R. A. Pfuetzner, A. Kuo, J. M. Gulbis, S. L. Cohen, B. T. Chait, and R. MacKinnon. 1998. The structure of the potassium channel: molecular basis of K^+ conduction and selectivity. *Science.* 280:69–77.

Galli, A., R. D. Blakely, and L. J. DeFelice. 1996. Norepinephrine transporters have channel modes of conduction. *Proc. Natl. Acad. Sci. U.S.A.* 93:8671–8676.

Galli, A., R. D. Blakely, and L. J. DeFelice. 1998. Patch-clamp and amperometric recordings from norepinephrine transporters: channel activity and voltage-dependent uptake. *Proc. Natl. Acad. Sci. U.S.A.* 95: 13260–13265.

Galli, A., C. I. Petersen, M. deBlaquiere, R. D. Blakely, and L. J. DeFelice. 1997. *Drosophila* serotonin transporters have voltage-dependent uptake coupled to a serotonin-gated ion channel. *J. Neurosci.* 17:3401–3411.

Gu, H., S. C. Wall, and G. Rudnick. 1994. Stable expression of biogenic amine transporters reveals differences in inhibitor sensitivity, kinetics, and ion dependence. *J. Biol. Chem.* 269:7124–7130.

Gu, H., S. C. Wall, and G. Rudnick. 1996. Ion coupling stoichiometry for the norepinephrine transporter in membrane vesicles from stably transfected cells. *J. Biol. Chem.* 271:6911–6916.

Hille, B. 2001. Ion Channels of Excitable Membranes. 3rd Edition. Sinauer Associates, Sunderland, MA.

Hille, B., and W. Schwarz. 1978. Potassium channels as multi-ion single-file pores. *J. Gen. Physiol.* 72.:409–442.

Hirai, T., J. Heymann, D. Shi, R. Sarker, P. Maloney, and S. Subramaniam. 2002. Three-dimensional structure of a bacterial oxalate transporter. *Nature Struct. Biol.* 9:1–4.

Hodgkin, A. L., and R. D. Keynes. 1955. The potassium permeability of a giant nerve fibre. *J. Physiol.* 128:61–88.

Iversen, L. L. 1971. Role of transmitter uptake mechanisms in synaptic neurotransmission. *Br. J. Pharmacol.* 41:571–591.

Johnson, R. A., A. J. Eshleman, T. Meyers, K. A. Neve, and A. Janowsky. 1998. [^{3}H]Substrate- and cell-specific effects of uptake inhibitors on human dopamine and serotonin transporter-mediated efflux. *Synapse.* 30:97–106.

King, E. L., and C. Altman. 1956. A schematic method of deriving the rate laws for enzyme-catalyzed reactions. *J. Phys. Chem.* 60:1375–1378.

Keyes, S. R., and G. Rudnick. 1982. Coupling of transmembrane proton gradients to platelet serotonin transport. *J. Biol. Chem.* 257:1172–1176.

Läuger, P. 1991. Electrogenic Ion Pumps. Sinauer Associates, Sunderland, MA.

Lin, F., H. A. Lester, and S. Mager. 1996. Single-channel currents produced by the serotonin transporter and analysis of a mutation affecting ion permeation. *Biophys. J.* 71:3126–3135.

Minta, A., and R. Y. Tsien. 1989. Fluorescent indicators of cytosolic sodium. *J. Biol. Chem.* 264:19449–19457.

Nelson, P. J., and G. Rudnick. 1979. Coupling between platelet 5-hydroxytryptamine and potassium transport. *J. Biol. Chem.* 254:10084–10089.

Parry, B. L. 2001. The role of central serotonergic dysfunction in the aetiology of premenstrual dysphoric disorder: therapeutic implications. *CNS Drugs.* 15:277–285.

Petersen, C. I. and L. J. DeFelice. 1999. Ionic interactions in the *Drosophila* serotonin transporter identify it as a serotonin channel. *Nat. Neurosci.* 2:605–610.

Qian, Y., A. Galli, S. Ramamoorthy, S. Risso, L. J. DeFelice, and R. D. Blakely. 1997. Protein kinase C activation regulates human serotonin transporters in HEK-293 cells via altered cell surface expression. *J. Neurosci.* 17:45–57.

Ramamoorthy, S., A. L. Bauman, K. R. Moore, H. Han, T. Yang-Feng, A. S. Chang, V. Ganapathy, and R. D. Blakely. 1993. Antidepressant- and cocaine-sensitive human serotonin transporter: molecular cloning, expression, and chromosomal localization. *Proc. Natl. Acad. Sci. U.S.A.* 90:2542–2546.

Rudnick, G., and S. C. Wall. 1992. The molecular mechanism of "ecstasy" [3,4-methylenedioxy methamphetamine (MDMA)]: serotonin transporters are targets for MDMA-induced serotonin release. *Proc. Natl. Acad. Sci. U.S.A.* 89:1817–1821.

Rudnick, G., and P. J. Nelson. 1978. Platelet 5-hydroxytryptamine transport, an electroneutral mechanism coupled to potassium. *Biochemistry.* 17:4739–4742.

Scholze, P., H. H. Sitte, and E. A. Singer. 2001. Substantial loss of substrate by diffusion during uptake in HEK-293 cells expressing neurotransmitter transporters. *Neurosci. Lett.* 309:173–176.

Sitte, H. H., B. Hiptmair, J. Zwach, C. Pifl, E. A. Singer, and P. Scholze. 2001. Quantitative analysis of inward and outward transport rate in cells stably expressing the cloned human serotonin transporter: inconsistencies with the hypothesis of facilitated transport. *Mol. Pharm.* 59: 1129–1137.

Sitte, H. H., P. Scholze, P. Schloss., C. Pifl, and E. A. Singer. 2000. Characterization of carrier-mediated efflux in human embryonic kidney 293 cells stably expressing the rat serotonin transporter: a superfusion study. *J. Neurochem.* 74:1317–1324.

Stein, W. D. 1986. Transport and Diffusion across Cell Membranes. Academic Press Inc, San Diego, CA.

Su, A., S. Mager, S. L. Mayo, and H. A. Lester. 1996. A multi-substrate single-file model for ion-coupled transporters. *Biophys. J.* 70:762–777.

Tatsumi, M., K. Groshan, R. D. Blakely, and E. Richelson. 1997. Pharmacological profile of antidepressants and related compounds at human monoamine transporters. *Eur. J. Pharmacol.* 340:249–258.